Ultrafast Electrochemical Lithiation of Individual Si Nanowire Anodes

Xiao Hua Liu,[†] Li Qiang Zhang,[‡,||] Li Zhong,[‡] Yang Liu,[†] He Zheng,[‡,¶] Jiang Wei Wang,[‡] Jeong-Hyun Cho,[§] Shadi A. Dayeh,[§] S. Tom Picraux,[§] John P. Sullivan,[†] Scott X. Mao,[‡] Zhi Zhen Ye,[||] and Jian Yu Huang*,[†]

[†]Center for Integrated Nanotechnologies, Sandia National Laboratories, Albuquerque, New Mexico 87185, United States

[‡]Department of Mechanical Engineering and Materials Science, University of Pittsburgh, Pittsburgh, Pennsylvania 15261, United States

[§]Center for Integrated Nanotechnologies, Los Alamos National Laboratory, Los Alamos, New Mexico 87545, United States

[||]State Key Laboratory of Silicon Materials, Department of Materials Science and Engineering, Zhejiang University, Hangzhou, 310027, People's Republic of China

[¶]School of Physics and Technology, Center for Electron Microscopy and MOE Key Laboratory of Artificial Micro- and Nanostructures, Wuhan University, Wuhan 430072, China

S Supporting Information

ABSTRACT: Using advanced in situ transmission electron microscopy, we show that the addition of a carbon coating combined with heavy doping leads to record-high charging rates in silicon nanowires. The carbon coating and phosphorus doping each resulted in a 2 to 3 orders of magnitude increase in electrical conductivity of the nanowires that, in turn, resulted in a 1 order of magnitude increase in charging rate. In addition, electrochemical solid-state amorphization (ESA) and inverse ESA were directly observed and characterized during a two-step phase transformation process during lithiation: crystalline silicon (Si) transforming to amorphous lithium—silicon (Li$_x$Si) which transforms to crystalline Li$_{15}$Si$_4$ (capacity 3579 mAh·g^{-1}). The ultrafast charging rate is attributed to the nanoscale diffusion length and the improved electron and ion transport. These results provide important insight in how to use Si as a high energy density and high power density anode in lithium ion batteries for electrical vehicle and other electronic power source applications.

KEYWORDS: Silicon nanowire, lithium ion battery, fast lithiation, carbon coating, doping
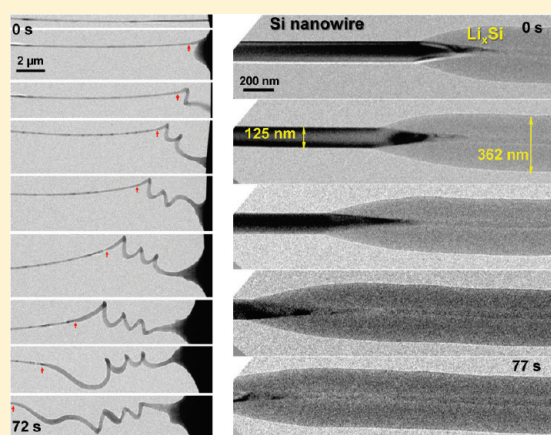
Doping and carbon coating are two important techniques to improve the energy capacity and rate performance of lithium ion batteries (LIBs). Chiang et al. reported a ~10^8 orders of magnitude electronic conductivity improvement in LiFePO$_4$ by metal doping, which highlights the potential of LiFePO$_4$ as an important cathode material for LIBs with high energy density.[1] Ravet et al. contended later that it may be the carbon coating that leads to the dramatic increase of electronic conductivity,[2] with the debate still ongoing.[3] We recently demonstrated a nanoscale open cell electrochemical device that operates inside a transmission electron microscope (TEM), allowing real-time studies of the charging/discharging behavior of individual nanowire electrodes.[4] This provides a unique opportunity to investigate the carbon coating and doping effects on the lithiation behavior of Si nanowires.[5−11] Individual Si nanowires were either undoped (intrinsic), coated with carbon (C-coated) or heavily doped with phosphorus (P-doped), or first P-doped followed by C-coating and then subjected to in situ electrochemical lithiation with real-time monitoring. Full lithiation of the nanowires was achieved in all of the latter three cases, but a record high charging rate was achieved only in the P-doped and C-coated nanowires. Individually, carbon coating and phosphorus

doping resulted in similar electrical conductivity improvement and, in turn, similar charging rate performance of the Si nanowires.

We constructed an electrochemical device consisting of a single Si nanowire anode, an ionic liquid electrolyte (ILE), and a LiCoO$_2$ cathode inside a TEM to enable in situ studies of the charging and discharging processes of silicon LIB anodes (see Supporting Information). Our experimental setup is shown in Figure 1a. Figure 1b shows a low magnification TEM image of the gap part of the nano-LIB. Charging and discharging experiments were conducted by potentiostatic holds with the anode at different potentials with respect to the cathode at room temperature (~300 K). For all experiments described hereafter, the potential applied to the Si nanowires with respect to the LiCoO$_2$ cathode was −4 V during charging and 0 V during discharging. Four types of Si nanowires were studied: undoped (intrinsic), C-coated, heavily P-doped, and C-coated plus P-doped.

Figure 2 shows the charging process of an intrinsic Si nanowire. When a potential of −4 V was applied, charging of the nanowire
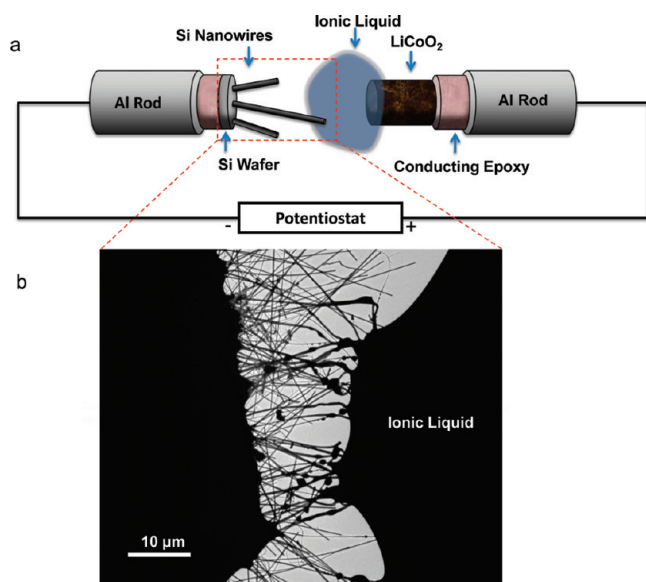
Figure 1. Experimental setup. (a) Schematic illustration of the electrochemical device. The Si wafer substrate supporting vertically oriented Si nanowires (anode) grown on the surface was cleaved and glued to an Al rod using conducting epoxy. A bulk $LiCoO_2$ film (cathode) on an Al foil was glued to another Al rod. A drop of the ionic liquid electrolyte was placed on the $LiCoO_2$ surface and the system loaded into the TEM. Inside the TEM, one of the Si nanowire electrodes was driven to approach the electrolyte covered $LiCoO_2$ cathode. A potential was applied with a potentiostat when contact was established. (b) Low magnification TEM image showing the gap part of the device. Many nanowires were bent and swelled after contacting the ILE and being charged. Some straight nanowires that were not contacting the electrolyte remained intact and undisturbed.

occurred. As the reaction front (marked by the red arrows) passed by, the nanowire diameter expanded immediately. As the leading edge of the reaction front propagated longitudinally down the nanowire axis, the lithiation front also proceeded progressively along the radial direction, i.e., from the surface to the center of the nanowire (Figure 2a−g and si_002.mov, si_003.mov in the Supporting Information). Electron diffraction patterns (EDPs) from the pristine and lithiated Si nanowires confirmed that the single crystalline Si (c-Si) nanowire was partially converted to an amorphous Li_xSi (a-Li_xSi) alloy (Figure 2h,i). After reaction, the nanowire appeared as a gray-contrast shell with a crystalline-contrast core. The c-Si core diameter decreased while the a-Li_xSi shell diameter increased (Figure 2j−n) progressing toward the right (toward the initiation point of the lithiation). Interestingly, the volume expansion occurred along the radial direction without detectable elongation, in marked contrast to the nearly isotropic volume expansion in SnO_2 nanowires during lithiation.[4] The total volume expansion was ∼300%, close to the theoretical maximum volume expansion.[12] Finally, the axial reaction front migration speed was slow for the intrinsic Si nanowires (Figure 2), being about 1.7 nm/s. A residual c-Si core was usually observed even after prolonged charging, possibly due to insufficient electron transport through the narrow c-Si core or poor electrical conductivity of the c-Si core due to surface charge depletion of nanosized wire, which limits the extent of the lithiation reaction.

Our observations are also consistent with the reported electrochemically driven solid-state amorphization (ESA) of Si.[13,14] We observed similar ESA in Si nanowires where a portion of their length was fully immersed in the electrolyte (Figure 3). Further

evidence for the electron conductivity limiting the extent of lithiation is suggested following comparison of the extent of lithiation near the middle (Figure 3i) and end (Figure 3j) of the immersed doped Si nanowire. Although both immersed in the bulk electrolyte, the extent of lithiation was higher near the electrolyte interface, suggesting that the reaction is not lithium diffusion limited, but rather limited by the supply of electrons from the unreacted electrode (left side of Figure 3).

Since poor electrical conductivity appears to hamper fast and full lithiation, it is interesting to see whether enhancements in the electrical conductivity change the charging behavior of Si nanowires. To improve the nanowire electrical conductivity, we grew heavily doped Si nanowires (phosphorus doped, P-doped), and we coated Si nanowires (intrinsic and heavily doped) with a layer of sputtered amorphous carbon, C-coated. The charging behavior of the heavily P-doped and C-coated Si nanowires is shown in Figure 4 and Figure 5, respectively. Figure 4 shows the microstructure changes and high charging rates of a P-doped Si nanowire (n-type). The pristine P-doped Si nanowire was single crystalline with a diameter of 170 nm, and its growth direction was [112] (Figure 4a,b). After 3240 s of charging, the nanowire was bent and the diameter expanded to 446 nm (Figure 4d). EDPs from multiple sites, either above or below the ILE surface, confirmed that the whole nanowire was converted to the same crystalline $Li_{15}Si_4$ (c-$Li_{15}Si_4$) phase (Figure 4f).[12,15,16] Figure 4g shows the simulated EDP for the c-$Li_{15}Si_4$ phase (a = 10.6852 Å, space group $I\bar{4}3d$) with intensity and indices in excellent agreement with our experimental results.

The microstructural evolution of a C-coated Si nanowire followed through two charging/discharging cycles (Figure 5) showed three similar features as observed for the P-doped Si nanowire: (1) fast charging; (2) large volume expansion; and (3) full lithiation to the c-$Li_{15}Si_4$ phase in the first charging process. Panels a−e of Figure 5 show morphology changes during cycling. Detailed structure evolution is shown in high-magnification TEM images (Figure 5g−k) and EDPs (Figures 5l−p). The pristine Si nanowire was straight and uniform, 100 nm in diameter, and its axis oriented along the [112] direction (Figure 5a,g,l). The carbon coating was amorphous and about 3 nm thick (inset of Figure 5g). After the first charging process, which required 221 s, the nanowire was fully lithiated to c-$Li_{15}Si_4$ (Figure 5b,m), and the diameter expanded to 303 nm (Figure 5h). The charging rate of the C-coated Si nanowire during the first charging process (determined by the velocity of the reaction front) was at least 10 times faster than the noncoated intrinsic Si nanowires. Furthermore, the carbon layer expanded from 3 to ∼13 nm during the first charging (Figure 5g,h), suggesting that the carbon layer was also becoming lithiated and/or porous or modified by the formation of a solid-electrolyte interface (SEI) layer through electrolyte decomposition. After the first discharging process, the c-$Li_{15}Si_4$ nanowire was delithiated to amorphous silicon (a-Si, Figure 5c,i,n).[12,15,17−19] As a result, shrinkage occurred along both radial and axial directions (Figure 5c), together accounting for a volume contraction of ∼55%. After the second charging process, volume expansion along both radial and axial directions was again observed (Figure 5d,j), but EDP revealed that an amorphous Li−Si alloy, a-Li_xSi, was the main lithiated product (Figure 5o), in contrast to the c-$Li_{15}Si_4$ phase observed following the first charging cycle. After the second discharging process, a-Si was obtained again and the volume shrank by ∼34% (Figure 5e,k,p). Figure 5f shows the typical view of the C-coated Si nanowire after deimmersion
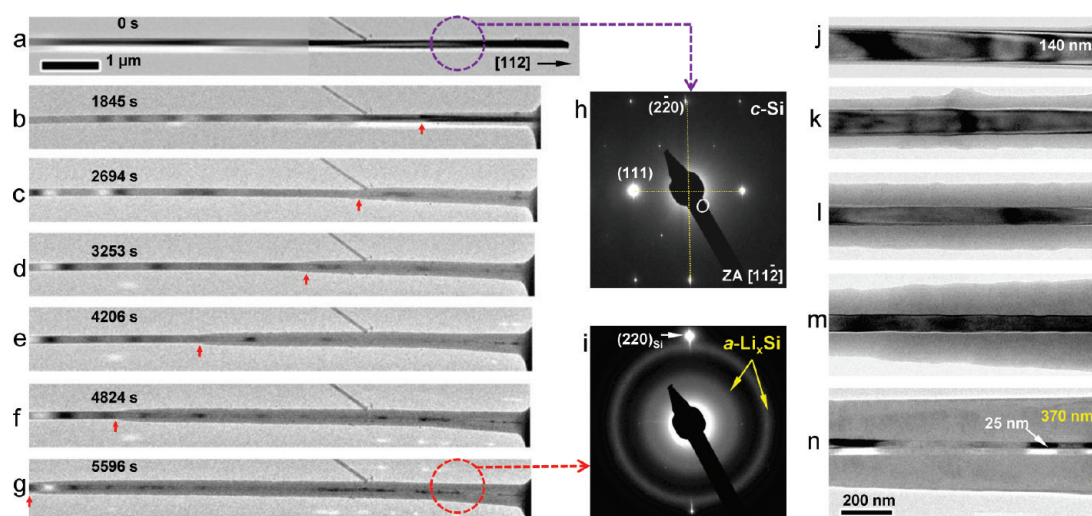
Figure 2. Microstructural evolution of an intrinsic silicon nanowire during lithiation. (a) Pristine straight Si nanowire with a uniform diameter of 140 nm. (b–g) Time-lapse TEM image series showing the morphology change during charging. The potential applied to the Si nanowire was −4 V against the LiCoO$_2$ cathode. Volume expansion occurred instantaneously as the reaction front (marked by the red arrows) propagated from the nanowire tip toward its base at an average rate of 1.7 nm/s. (h) EDP from the pristine nanowire showing the single crystalline silicon (c-Si). (i) EDP from the lithiated nanowire showing an amorphous Li$_x$Si (a-Li$_x$Si) alloy. The sharp spots were from the residual c-Si core. (j–n) High-magnification TEM images showing that radial lithiation resulted in a core–shell structure. The c-Si core became thinner, from the original 140 nm down to 25 nm, while the nanowire thickened to 370 nm, indicating more Si was converted to a Li$_x$Si alloy. The radial lithiation seemed to cease despite prolonged lithiation time, suggesting the reaction was limited due to insufficient electron supply from the very small c-Si core.
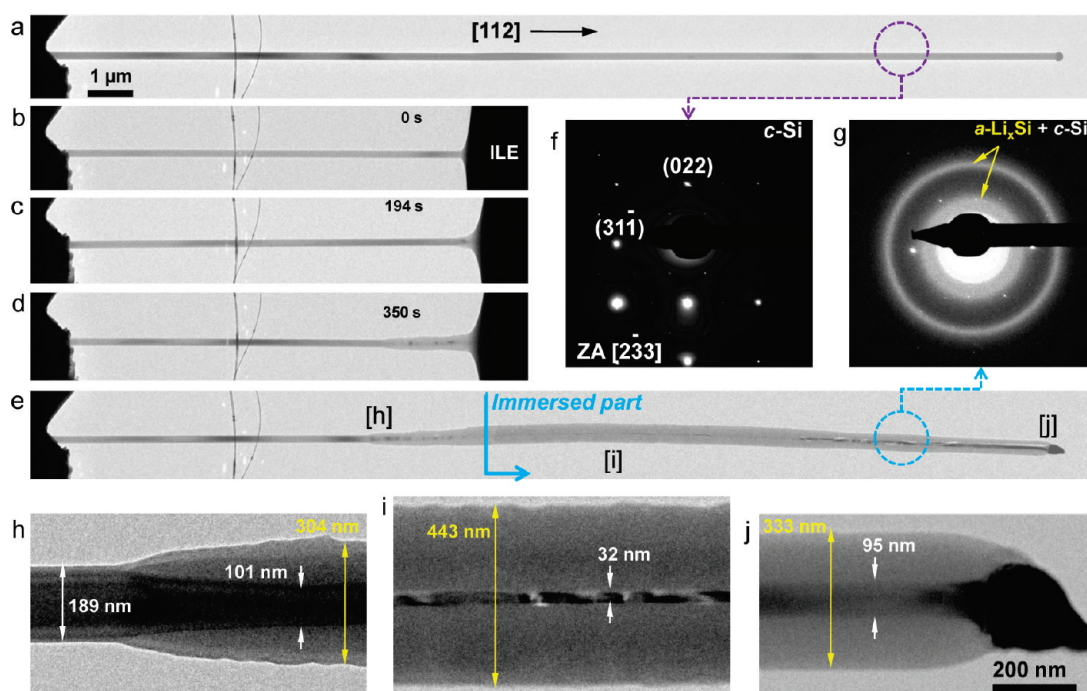
Figure 3. Electrochemically driven solid-state amorphization (ESA) process occurring above and below the electrolyte surface. (a) A pristine phosphorus-doped (P-doped) Si nanowire showing a straight shape and uniform diameter. (b–d) Morphology evolution during the charging process. The reaction front emerged from above the ILE surface (c) and proceeded toward the nanowire base (d). (e) Morphology of the nanowire pulled out of the ILE. The whole immersed part was swelled and the Au cap was elongated. Note that the expansion was not uniform for the lithiated part. (h–j) Magnified view of the reaction front (h), middle of the lithiated part (i), and nanowire tip (j). The tapering crystalline silicon (c-Si) core indicated that lithiation was proceeding from the surface toward the center (h). The residual c-Si was thinner in (i) than that in (j), indicating a lower degree of lithiation at the nanowire tip, though both were flooded in the ILE during lithiation, probably due to insufficient electron supply to the tip (j). (f, g) Electron diffraction patterns showing that the single crystalline pristine nanowire (f) was partially converted to an amorphous Li$_x$Si (a-Li$_x$Si) alloy (g).

from the ILE. Typically, there was a large chunk of gelled electrolyte adhered to the formerly immersed part of the nanowire

(Figure 5f), which is very different from the clean surface of the P-doped Si nanowire following deimmersion (Figure 4e). It is
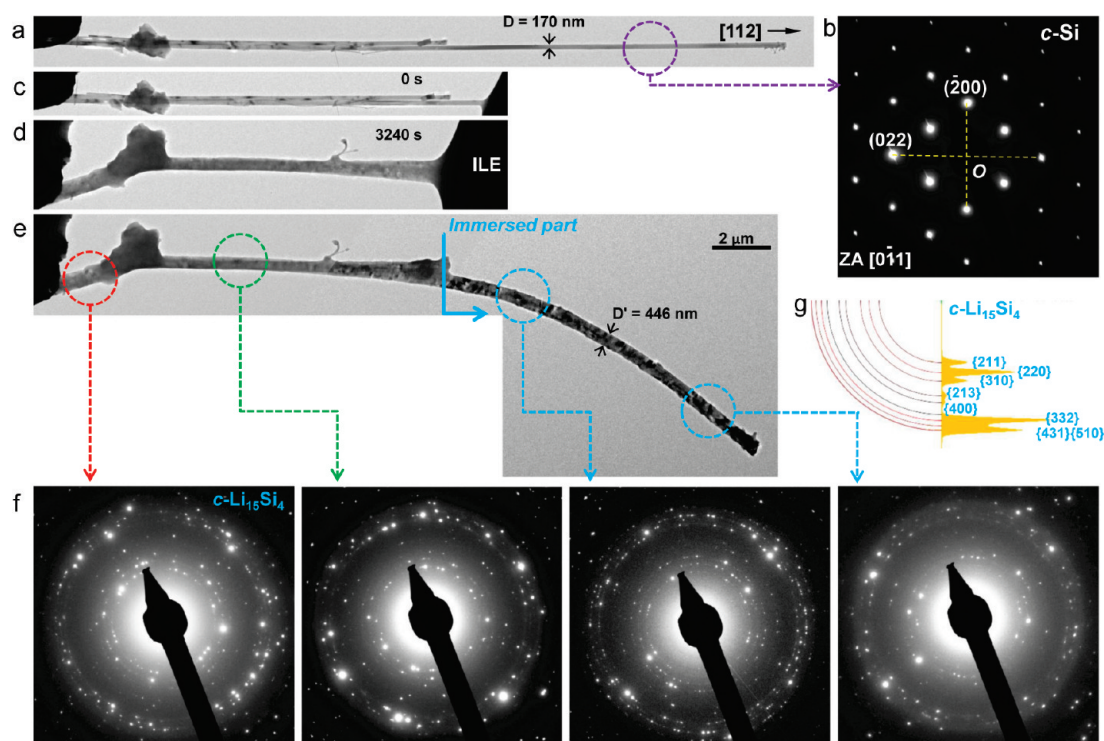
Figure 4. Fast and full lithiation of a P-doped silicon nanowire. (a) Pristine P-doped Si nanowire and corresponding EDP (b). (c, d) Swelled nanowire after 3240 s of charging. (e) Morphology of the nanowire after deimmersion from the electrolyte. The whole nanowire showed a uniform crystalline contrast without the core–shell structure as seen in Figure 2 for the intrinsic Si nanowire. The diameter increased from 170 to 446 nm without elongation. (f) EDPs from different sites confirming the formation of crystalline $Li_{15}Si_4$ (c-$Li_{15}Si_4$) phase along the whole nanowire. (g) Simulated EDP for polycrystalline $Li_{15}Si_4$ with indexing and intensity.

suggested that the carbon coating might not only provide an additional electron transport path but also alter the SEI formation or reaction kinetics.[5,7,20]

Figure 5g–k show close views of the morphology changes of the nanowire following the two complete sets of charging and discharging. The carbon layer was visible at all stages. Apparently, the most significant change took place during the first charging process. This was true for all Si nanowires investigated in this study. This observation would also be consistent with the formation of an SEI layer on or embedded within the carbon coating, as this solid electrolyte phase is typically observed to grow to a self-limiting thickness following the first or first few charging cycles. The carbon coating enhanced the charging rate, but it did not suppress the radial volume expansion, probably due to its thin and amorphous nature. Nevertheless, our results clearly indicated that higher charging rates were achieved by either phosphorus doping or carbon coating, with the reaction front migration speed being 7.7 and 77.6 nm/s for the above two examples (Figures 4 and 5), which is in contrast to the 1.7 nm/s of the intrinsic Si nanowire (Figure 2). Another key charging behavior difference between the intrinsic and C-coated or P-doped Si nanowire was the complete transition to the c-$Li_{15}Si_4$ in the latter two cases, at least during the first charging process, rather than the partial conversion to the a-Li_xSi alloy in the former.

To test whether we can improve the charging rate further, the P-doped Si nanowire was coated with carbon and subjected to charging. Surprisingly, a further increase in the charging rate was observed (Figure 6a–i, Movies si_004.mov to si_007.mov in the Supporting Information). At this very high axial charging rate,

213 nm/s on average for this nanowire, spiral and twisting motion of the lithiated nanowire occurred. Such a nanowire was lithiated to an amorphous phase nearly immediately (Figure 6j) and then to a crystalline phase as the reaction front swept over. The crystalline phase was confirmed to be c-$Li_{15}Si_4$ (Figures 6k–m). The time required for fully charging such P-doped and C-coated Si nanowires along their entire length was about 1–5 min and along their entire diameter about 1 s.

Figure 7a compares the axial charging rates (defined as the reaction front speed in the first charging process) for the four types of Si nanowires: (1) intrinsic, (2) P-doped, (3) C-coated, and (4) C-coated and P-doped. The average charging rates were 2.3, 20.5, 27.5, and 117.4 nm/s, respectively. It is clear that either P-doping or C-coating can improve the first cycle charging rate by 1 order of magnitude with respect to the intrinsic Si nanowires, and the rate can be improved further by another order of magnitude by combining P-doping and C-coating (see Supporting Information for details of the conductivity measurements). Figure 7b shows the schematic illustration of the ultrafast charging of the P-doped and C-coated Si nanowire shown in panels a–i of Figure 6. In a flooded electrolyte geometry where lithiation proceeds radially, the 146 nm thick Si nanowire can be charged in 0.343 s, converting the pristine c-Si nanowire to c-$Li_{15}Si_4$, corresponding to a charging rate of $\sim$37600 $A \cdot g^{-1}$ (or 10500C, with 1C = 3579 $mA \cdot g^{-1}$ for the Si $\rightarrow Li_{15}Si_4$ alloying reaction). This record high rate far exceeds any rates achieved for Si electrodes with more mass load reported in the literature, for instance, 6.8 $A \cdot g^{-1}$ for a-Si/c-Si core–shell nanowires[18] or $\sim$60 $A \cdot g^{-1}$ (originally claimed 30C) for a P-doped a-Si thin film.[21] Although it is hard to directly compare
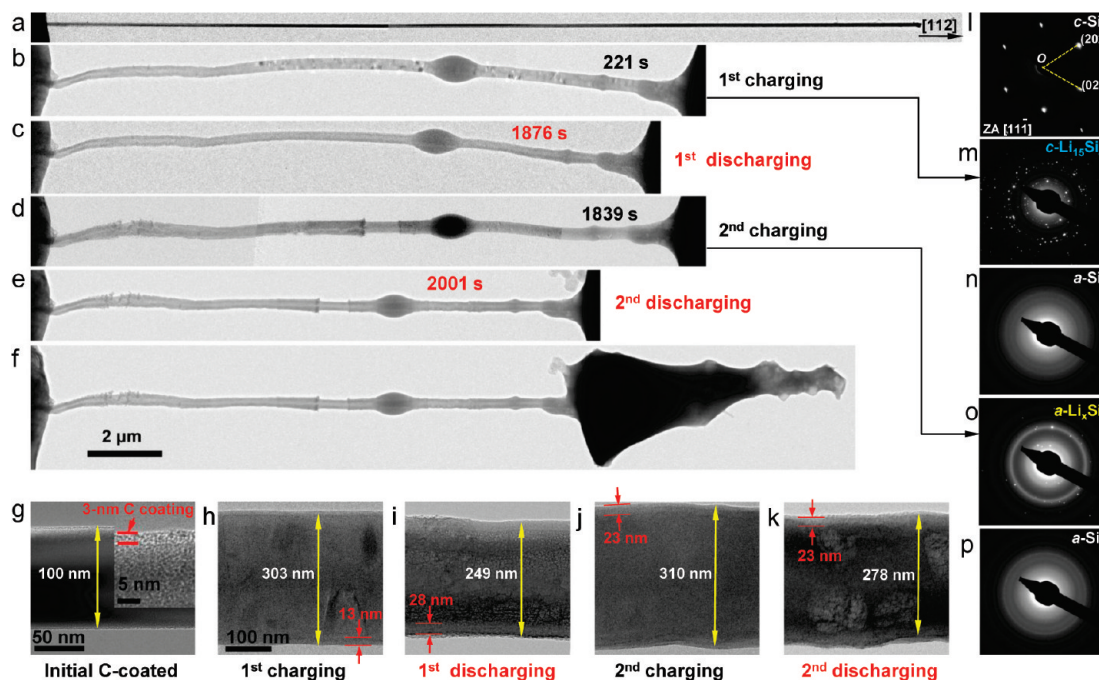
Figure 5. Fast and full lithiation of a carbon-coated silicon nanowire. (a−f) Morphology changes of a carbon-coated Si nanowire in two charging/discharging cycles. The microstructure evolution is shown in high magnification images (g−k) and corresponding EDPs (l−p). The carbon coating on the pristine intrinsic Si nanowire was 3 nm thick (g). The nanowire was fully charged to the c-Li$_{15}$Si$_4$ phase in 221 s (b, h, m). Upon discharging, amorphous silicon (a-Si) was formed (c, i, n). Amorphous Li$_x$Si rather than c-Li$_{15}$Si$_4$ was formed after the second charging process (d, j, o). After the second discharge process, a-Si was obtained again (e, k, p). Volume changes along both radial and longitudinal directions were seen after the first charging process (c−e), probably due to the isotropic nature of the amorphous phases involved (n−p). The carbon layers also participated in the reaction, as their thickness was increased after charging, and decreased after discharging (g−k). The diameter variation along the nanowire in (d−f) was due to electron-beam induced decomposition of the lithiated nanowires when imaged at high magnifications. Following deimmersion from the electrolyte, a large chunk of gelled electrolyte was seen in the region that was immersed (f), which was a typical result for carbon-coated samples.

the rate performance in different device configurations, i.e., bulk electrodes or single nanowire electrodes, our in situ tests on individual Si nanowires show great potential of making high-power Si electrodes. Surprisingly, the integrity of the nanowires charged at high rates was well-maintained, suggesting the great potential of using Si anodes for high power applications. The volume change was typically around 300% after the first charging process, regardless of the lithiation products (c-Li$_{15}$Si$_4$ or a-Li$_x$Si). This implies that for Si nanowires with facile strain accommodation,[17] formation of the crystalline Li$_{15}$Si$_4$ phase and resulting lithiation rate may not necessarily be worse than the amorphous phases (a-Li$_x$Si ↔ a-Si).[12,18]

Intrinsic Si is a poor electron conductor and is generally accepted to have a p-type doped character due to its acceptor-like surface states, creating electron deficiency throughout the whole nanowire diameter. This hinders fast lithiation rates which require high electron density to support Li ion reduction at the lithiation front (Li$_x$Si/Si interface). Figure 7c shows typical lithiated length (L) versus time (t) plots for the Si nanowires with different electrical conductivities. The L−t curve is parabolic for the intrinsic Si nanowire (Figure 7c, Figure S1 in the Supporting Information), while it shows linear $L ∝ t$ relationship for the other three types of Si nanowires with higher conductivity (Figure 7c). Figure 7d shows a schematic illustration depicting the kinetics for the intrinsic Si nanowire. Both electron and Li$^+$ ion fluxes are required for the interface reaction of lithiation; however, the Li$^+$ transport from a surface ILE layer is assumed to

be fast as the liquid electrolyte can conduct Li$^+$ quickly, thus not acting as a limiting factor for lithiation.

In the following, we present a qualitative explanation of the different L−t dependence in different type Si nanowires considered in this study. Assuming the lithiation rate is electron supply limited, given the original length L_0 of a pristine Si nanowire, the lithiation speed, dL/dt, is proportional to the current, $I(L)$

$$\frac{dL}{dt} \propto I(L) = \frac{V - V_0}{\rho_{Si}\frac{L_0 - L}{A_{Si}} + \rho_{Li_xSi}\frac{L}{A_{Li_xSi}}} = \frac{1}{b - 2aL} \quad (1)$$

where the applied bias, V, is constantly 4 V and V_0 is the potential drop across the lithiation front; the resistivity, ρ, and the area, A, of unreacted Si and lithiated Li$_x$Si alloy are treated as constants. The relation of dL/dt = $1/(b - 2aL)$ is obtained by merging all of the constants to two lumped positive constants a and b ($b > 2aL_0 > 0$). By using the boundary condition $L = 0$ ($t = 0$), the following L−t relation is achieved if the electron transport is the determining factor

$$t = -aL^2 + bL \quad (0 < L < L_0) \quad (2)$$

Equation 2 reproduces the parabolic curve observed for intrinsic Si nanowires (black curve in Figure 7c). As the lithiation proceeds, the unreacted segment becomes shorter and shorter; thus lithiation is accelerated, mainly due to decreasing IR potential drop and short electron transport length (Figure 7c). For the Si nanowires with
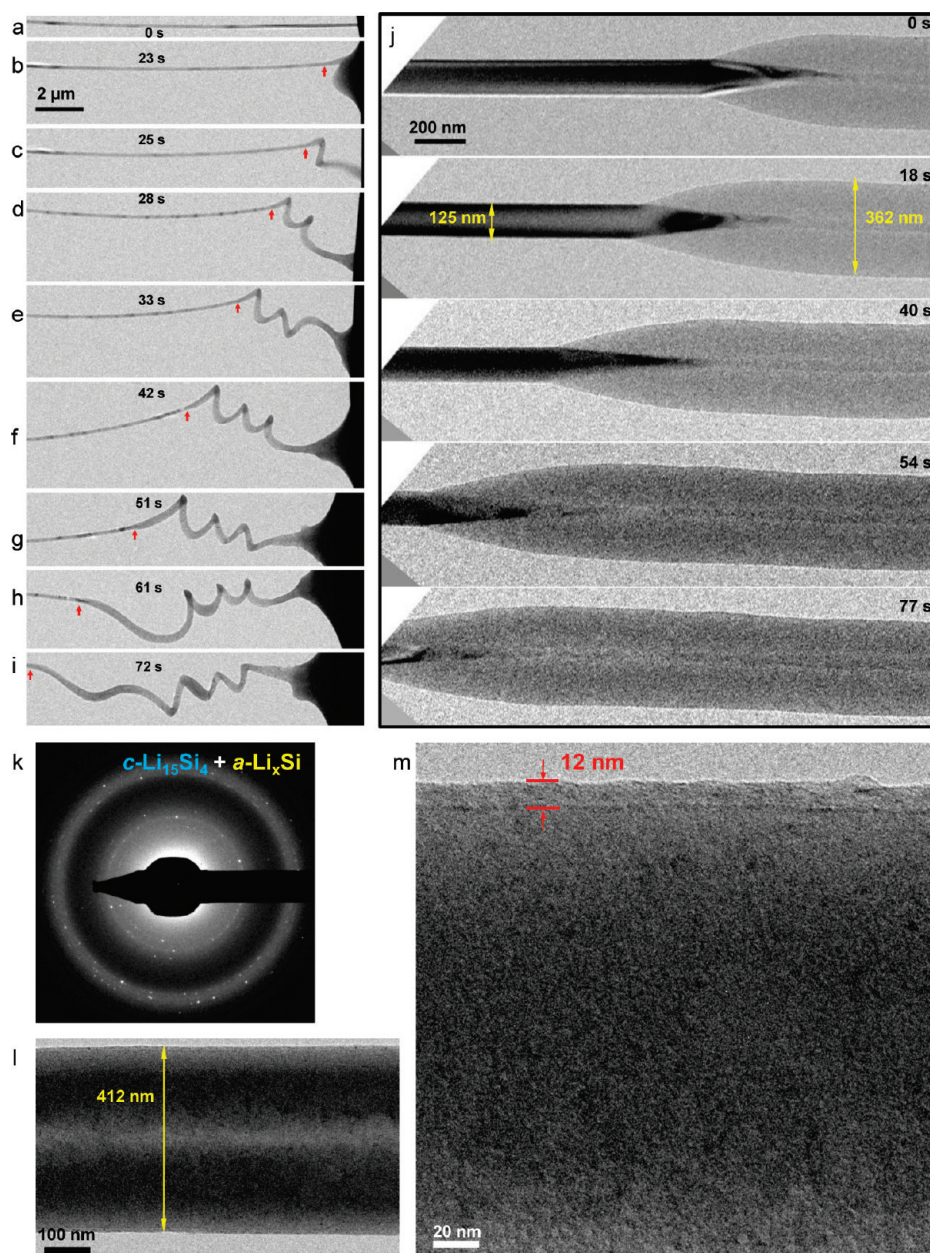
Figure 6. Ultrafast charging of carbon-coated and phosphorus-doped silicon nanowires. (a−i) Morphology evolution in 72 s after the bias was applied. The spiral shape was observed only at very high lithiation rates (reaction front marked by red arrows). The average speed for the reaction front was 213 nm/s. (j) High magnification time-lapse TEM images showing an immediate expansion after lithiation and the core−shell lithiation behavior. (k−m) Microstructure of the C-coated and P-doped Si nanowire shown in (j) after lithiation. (k) EDP showing coexistence of the crystalline $Li_{15}Si_4$ (c-$Li_{15}Si_4$) and a-Li_xSi phases. (l) Low magnification image of the lithiated part. (m) High-magnification image showing the contrast of nanocrystals dispersed in an amorphous matrix, consistent with the EDP (k). The carbon layer was also swelled from originally 3 to 12 nm after lithiation.

sufficiently high electrical conductivity, the kinetics is not limited by electron transport and is instead likely controlled by short-range interface reaction kinetics, giving a linear $L-t$ relation (green, red, and blue curves in Figure 7c). We also note that reaction does not seem to be long-range diffusion limited, which would give $L \sim t^{1/2}$ diffusion kinetics.

Finally, it is also worth noting that the c-$Li_{15}Si_4$ phase was the only crystalline phase formed in the lithiation of many different Si nanowires. No phase change occurred if the charging time or potential was increased. This brings up an important question as to what is the final lithiated alloy phase of Si at room temperature, as

this defines the practical maximum capacity of Si anodes. Some references claimed that the ultimate phase is the very high capacity $Li_{22}Si_5$ or $Li_{21}Si_5$ phases,[17,22] but identification of these phases based on the diffuse diffraction rings from an amorphous material was questionable.[17] Our identification of the lithiated phase is based on the sharp diffraction rings generated by the crystalline phase, rather than from diffuse diffraction rings, and this makes the identification very accurate and reliable. Consequently, our experimental results indicate that the maximum lithium storage in Si is 3.75 Li/Si atoms, meaning that the maximum energy storage capacity for Li in Si is 3579 mAh·g^{-1} rather than the widely believed 4200 mAh·g^{-1}.
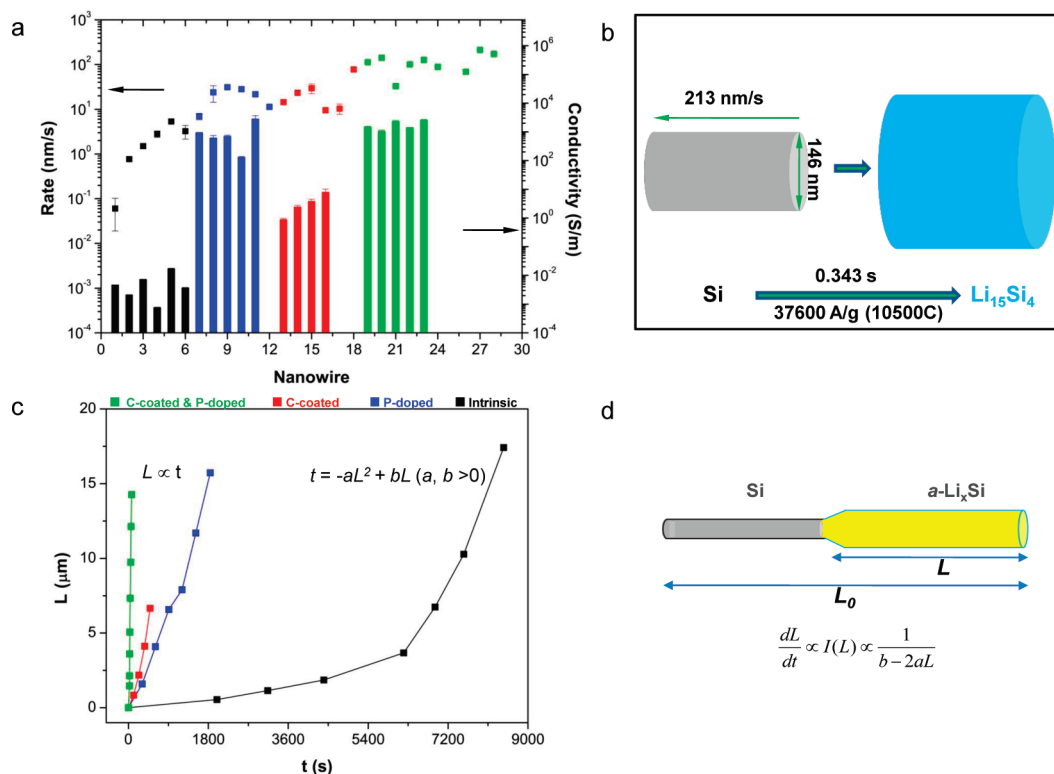
Figure 7. Lithiation speed and kinetics for different Si nanowires. (a) Comparison of reaction front propagation speeds and conductivities of the intrinsic, P-doped, C-coated, and C-coated on P-doped silicon nanowires. The average speeds were 2.3, 20.5, 27.5, and 117.4 nm/s, respectively, and the average conductivities were 5.95×10^{-3}, 1.05×10^{3}, 3.76, and 1.77×10^{3} S·m^{-1}, respectively, for the four samples mentioned in (a). The charging rate was improved by the enhanced electronic conductivity from doping and carbon coating. (b) Schematic illustration estimating the ultrafast charging of Si nanowires. Given the diameter of 146 nm and a lithiation rate of 213 nm/s for the nanowire shown in panels a—i of Figure 6, if we assume the active material (Si) was flooded in electrolyte (as in a real battery), the radial lithiation would be completed in 0.343 s, corresponding to a charging rate of 37600 A·g^{-1} or 10500 C (1C denoting 3579 mA·g^{-1} for full lithiation to the Li$_{15}$Si$_4$ phase). (c) Typical reaction front travel distance vs time ($L-t$) curves for the different Si nanowires. The curve was parabolic for the intrinsic Si nanowire, with increasing lithiation speed as the reaction proceeded. The curves were linear for the other three types of Si nanowires, indicating the lithiation was interface reaction controlled rather than diffusion controlled. (d) Schematic illustration showing the lithiation kinetics limited by insufficient electron supply for the intrinsic Si nanowires.

This result is consistent with that obtained from an in situ X-ray diffraction study.[23] However, the exact Li/Si ratio in the amorphous Li$_x$Si phase was not known, because the detailed atomic structure was not identified from the diffuse rings in the electron diffraction patterns. In the meantime, the lithiation current was too small to be measured due to the very small mass involved in the tests on individual nanowires, so determination of the Li content in the amorphous phase and Columbic efficiency will require future work of accurately measuring the current.

Conclusions. In summary, we demonstrated ultrafast and full electrochemical lithiation of individual Si nanowires by applying a carbon-coating, phosphorus-doping, or combining both doping and carbon coating. These results were obtained by direct real-time observation using in situ transmission electron microscopy with ionic liquid electrolytes. In contrast to the fast lithiation of doped or coated nanowires, lithiation of intrinsic Si nanowires was slow and incomplete, leading to the formation of an amorphous Li$_x$Si alloy. The C-coated and/or P-doped Si nanowires exhibited a charging rate 1—2 orders of magnitude faster, ultimately forming the crystalline Li$_{15}$Si$_4$ phase. The Si nanowires did not fracture despite the ultrahigh lithiation rates and ~300% volume expansion. These observations suggest that C-coated and/or P-doped Si nanowires show great promise for high power and high energy lithium ion batteries.

■ ASSOCIATED CONTENT

ⓢ Supporting Information. Experimental details for device construction, Si nanowire preparation, carbon coating, and electron microscopy. This material is available free of charge via the Internet at http://pubs.acs.org.

■ AUTHOR INFORMATION

Corresponding Author
*E-mail: jhuang@sandia.gov.

■ ACKNOWLEDGMENT

■ REFERENCES

(1) Chung, S. Y.; Bloking, J. T.; Chiang, Y. M. Electronically conductive phospho-olivines as lithium storage electrodes. *Nat. Mater.* **2002**, *1* (2), 123–128.

(2) Ravet, N.; Abouimrane, A.; Armand, M. From our readers - On the electronic conductivity of phosphoolivines as lithium storage electrodes. *Nat. Mater.* **2003**, *2* (11), 702–702.

(3) Hong, J.; Wang, C. S.; Dudney, N. J.; Lance, M. J. Characterization and performance of LiFePO$_4$ thin-film cathodes prepared with radio-frequency magnetron-sputter deposition. *J. Electrochem. Soc.* **2007**, *154* (8), A805–A809.

(4) Huang, J. Y.; Zhong, L.; Wang, C. M.; Sullivan, J. P.; Xu, W.; Zhang, L. Q.; Mao, S. X.; Hudak, N. S.; Liu, X. H.; Subramanian, A.; Fan, H. Y.; Qi, L. A.; Kushima, A.; Li, J. In Situ Observation of the Electrochemical Lithiation of a Single SnO$_2$ Nanowire Electrode. *Science* **2010**, *330* (6010), 1515–1520.

(5) Ishihara, T.; Nakasu, M.; Yoshio, M.; Nishiguchi, H.; Takita, Y. Carbon nanotube coating silicon doped with Cr as a high capacity anode. *J. Power Sources* **2005**, *146* (1−2), 161–165.

(6) Magasinski, A.; Dixon, P.; Hertzberg, B.; Kvit, A.; Ayala, J.; Yushin, G. High-performance lithium-ion anodes using a hierarchical bottom-up approach. *Nat. Mater.* **2010**, *9* (4), 353–358.

(7) Kong, M. H.; Noh, J. H.; Byun, D. J.; Lee, J. K. Electrochemical characteristics of phosphorus doped silicon and graphite composite for the anode materials of lithium secondary batteries. *J. Electroceram.* **2009**, *23* (2−4), 376–381.

(8) Kong, M. H.; Byun, D. J.; Lee, J. K. Effect of Phosphorus Doping into the Silicon as an Anode material for Lithium Secondary Batteries. *Adv. Mater. Processes* **2007**, *26−28*, 333–336.

(9) Zhou, S.; Liu, X. H.; Wang, D. W. Si/TiSi$_2$ Heteronanostructures as High-Capacity Anode Material for Li Ion Batteries. *Nano Lett.* **2010**, *10* (3), 860–863.

(10) Hertzberg, B.; Alexeev, A.; Yushin, G. Deformations in Si-Li Anodes Upon Electrochemical Alloying in Nano-Confined Space. *J. Am. Chem. Soc.* **2010**, *132* (25), 8548–8549.

(11) Ng, S.; Wang, J.; Wexler, D.; Konstantinov, K.; Guo, Z.; Liu, H. Highly reversible lithium storage in spheroidal carbon-coated silicon nanocomposites as anodes for lithium-ion batteries. *Angew. Chem., Int. Ed.* **2006**, *45*, 6896–6899.

(12) Obrovac, M. N.; Krause, L. J. Reversible cycling of crystalline silicon powder. *J. Electrochem. Soc.* **2007**, *154* (2), A103–A108.

(13) Limthongkul, P.; Jang, Y. I.; Dudney, N. J.; Chiang, Y. M. Electrochemically-driven solid-state amorphization in lithium-silicon alloys and implications for lithium storage. *Acta Mater.* **2003**, *51* (4), 1103–1113.

(14) Limthongkul, P.; Jang, Y. I.; Dudney, N. J.; Chiang, Y. M. Electrochemically-driven solid-state amorphization in lithium-metal anodes. *J. Power Sources* **2003**, *119*, 604–609.

(15) Obrovac, M. N.; Christensen, L. Structural changes in silicon anodes during lithium insertion/extraction. *Electrochem. Solid-State Lett.* **2004**, *7* (5), A93–A96.

(16) Chevrier, V. L.; Zwanziger, J. W.; Dahn, J. R. First principles study of Li-Si crystalline phases: Charge transfer, electronic structure, and lattice vibrations. *J. Alloys Compd.* **2010**, *496* (1−2), 25–36.

(17) Chan, C. K.; Peng, H. L.; Liu, G.; McIlwrath, K.; Zhang, X. F.; Huggins, R. A.; Cui, Y. High-performance lithium battery anodes using silicon nanowires. *Nat. Nanotechnol.* **2008**, *3*, 31–35.

(18) Cui, L. F.; Ruffo, R.; Chan, C. K.; Peng, H. L.; Cui, Y. Crystalline-amorphous core-shell silicon nanowires for high capacity and high current battery electrodes. *Nano Lett.* **2009**, *9* (1), 491–495.

(19) Kasavajjula, U.; Wang, C.; Appleby, A. Nano- and bulk-silicon-based insertion anodes for lithium-ion secondary cells. *J. Power Sources* **2007**, *163*, 1003–1039.

(20) Yang, X. Q.; McBreen, J.; Yoon, W. S.; Yoshio, M.; Wang, H. Y.; Fukuda, K.; Umeno, T. Structural studies of the new carbon-coated silicon anode materials using synchrotron-based in situ XRD. *Electrochem. Commun.* **2002**, *4* (11), 893–897.

(21) Takamura, T.; Ohara, S.; Uehara, M.; Suzuki, J.; Sekine, K. A vacuum deposited Si film having a Li extraction capacity over 2000 mAh/g with a long cycle life. *J. Power Sources* **2004**, *129* (1), 96–100.

(22) Kang, K.; Lee, H. S.; Han, D. W.; Kim, G. S.; Lee, D.; Lee, G.; Kang, Y. M.; Jo, M. H. Maximum Li storage in Si nanowires for the high capacity three-dimensional Li-ion battery. *Appl. Phys. Lett.* **2010**, *96* (5), 053110.

(23) Li, J.; Dahn, J. R. An in situ X-ray diffraction study of the reaction of Li with crystalline Si. *J. Electrochem. Soc.* **2007**, *154* (3), A156–A161.